frontiers in Materials

ORIGINAL RESEARCH
published: 03 March 2020
doi: 10.3389/fmats.2020.00038

Flexible Magnetostrictive Nanocellulose Membranes for Actuation, Sensing, and Energy Harvesting Applications

Aleksey Yermakov[1], Andrew Thompson[1], Christopher Coaty[2,3], Ronald Sabo[2], Chiu Tai Law[4] and Rani Elhajjar[5]*

[1] Department of Mechanical Engineering, University of Wisconsin – Milwaukee, Milwaukee, WI, United States, [2] USDA Forest Products Laboratory, Madison, WI, United States, [3] Department of NanoEngineering, University of California, San Diego, La Jolla, CA, United States, [4] Department of Electrical Engineering and Computer Science, University of Wisconsin – Milwaukee, Milwaukee, WI, United States, [5] Departments of Civil Engineering and Environmental and Materials Science, University of Wisconsin – Milwaukee, Milwaukee, WI, United States

Magnetostrictive composite known as magnetostrictive nanocellulose membrances (MNMs) were fabricated by embedding Terfeonol-D particles into cellulose nanofibers (CNFs). MNMs inherit flexibility and biodegradability from CNF while exhibiting magnetomechanical responses; as such, the valuable rare-earth (Terfenol-D) particles can be recycled. Various orientations of the Terfenol-D particles were induced in the MNMs, and those with in-plane alignment showed the strongest magnetostrictive effect but the lowest Villari effect. Materials with such a unique combination of properties dovetail nicely with Internet of Things that require ubiquitous sensing, actuation, and energy harvesting in one package.

Keywords: magnetostrictive composite, cellulose nanofiber, terfenol-D, Villari effect, magnetostriction

OPEN ACCESS

Edited by:
Seunghwa Ryu,
Korea Advanced Institute of Science & Technology (KAIST), South Korea

Reviewed by:
Fumio Narita,
Tohoku University, Japan
Domenico De Tommasi,
Politecnico di Bari, Italy

****Correspondence:***
Chiu Tai Law
lawc@uwm.edu

Specialty section:
This article was submitted to Mechanics of Materials, a section of the journal Frontiers in Materials

Received: *10 October 2019*
Accepted: *03 February 2020*
Published: *03 March 2020*

Citation:
Yermakov A, Thompson A, Coaty C, Sabo R, Law CT and Elhajjar R (2020) Flexible Magnetostrictive Nanocellulose Membranes for Actuation, Sensing, and Energy Harvesting Applications. Front. Mater. 7:38. doi: 10.3389/fmats.2020.00038

INTRODUCTION

Cellulose nanofibers (CNFs) are one class of natural fibers that have resulted in structures with remarkable mechanical properties enabling numerous potential applications, including substrates for flexible electronics, separation membranes, acoustic membranes, aerogels, medical scaffolding, and composite reinforcement (Saito et al., 2009; Siró and Plackett, 2010; Qamhia et al., 2013; Zheng et al., 2013; Sabo et al., 2016). The crystalline units of cellulose have impressive tensile strength and modulus of 10 and 140 GPa, respectively (Moon et al., 2011). Randomly oriented films of CNFs have shown tensile strength and modulus of more than 200 MPa and 20 GPa respectively, and oriented CNF films have shown even higher mechanical properties (Saito et al., 2009; Sehaqui et al., 2012; Qing et al., 2013). CNF films also exhibit high transparency, good flexibility, and high barrier properties. Such materials offer exciting potential for various devices, such as the matrix for the sensors, actuators, and energy harvesters being proposed here.

Several researchers have explored the possibility of inducing magnetic properties in nanocellulose materials but none have considered how to fabricate nanocellulose materials with magnetostrictive properties. Olsson et al. were able to make magnetic aerogels and nanopaper with cellulose nanofibrils as templates by facilitating the growth of ferromagnetic cobalt ferrite nanoparticles (Olsson et al., 2010). Other attempts have also shown the ability to incorporate

magnetic particles with cellulose materials by co-precipitation methods (Chia et al., 2008, 2009; Small and Johnston, 2009). In this study we propose a class of flexible materials for sensing, actuation and power generation. The proposed flexible magnetostrictive nanocellulose membranes (MNMs) can overcome the inherent deficiencies in piezoceramics such as brittleness (Zheng et al., 2003), high toxicity in lead based PZT (Zheng et al., 2003; Saito et al., 2004), low energy conversion efficiency (Roundy et al., 2003; Richards et al., 2004), inability to operate under long life cycles without the issues of depolarization (Franke et al., 1998; Anton et al., 2011; Bove et al., 2012), and the lack of flexibility to operate under high strong ambient vibrations (Jiang and Cross, 1993; Gruverman et al., 1996). The MNMs in this work consist of a composite material made of magnetostrictive particles and a CNF matrix. These MNMs are a novel class of magnetomechanical materials that are potentially recyclable with superior properties that are conducive for fabrication of sensors, actuators, and energy harvesters.

The structure of the CNFs provides an excellent substrate for magnetostrictive materials necessary for flexible sensors and devices. Magnetostriction is the property referring to the change in shape or dimensions during the process of magnetization as the magnetic field changes. The Joule effect describes the change in length owing to a change in the magnetization state of the material. Consequently, the magnetic field can be used to actuate or morph the flexible MNM. Conversely, a mechanical stress will change the magnetic susceptibility of a material through the inverse magnetostrictive effect (also known as the Villari effect). Since the MNM is expected to respond to changes in the external mechanical stresses by changing its magnetic domains, time varying stresses acting on these materials can induce voltage in coil(s), which can then be used to deliver electrical power to a load.

Sensors and energy harvesting devices have a need for materials with high energy densities and fast response times. Compared to piezoelectric materials, magnetostrictive materials have advantages, higher strain to failure and power density, for high power applications at low frequencies. These materials have been used in various devices and systems, such as sonars (Moffett et al., 1991; Claeyssen et al., 1997; Goldie et al., 1999), energy harvesting (Staley and Flatau, 2005; Wang and Yuan, 2008; Li et al., 2010; Ueno and Yamada, 2011), vibration control (Goodfriend and Shoop, 1992; Moon et al., 2007; Wang and Zhou, 2013) and position control (Fenn et al., 1996; Olabi and Grunwald, 2008). However, most bulk magnetostrictive materials are expensive owing to their rare earth metal ingredients. Their lack of ductility (Duenas and Carman, 2000) has hindered the fabrication of devices with complex shapes and ushered in proposals for various magnetostrictive polymer composites (Elhajjar et al., 2018).

In this study, key magnetomechanical properties required by actuators, sensors, and energy harvesters are examined. The experiments performed entail incorporating Terfenol-D particles into cellulose nanofibril films and evaluating the response of the materials to a magnetic field and mechanical stress. Unimorph films are examined for their actuation ability. Also the potential of composite films in converting mechanical energy to magnetic energy is explored by measuring changes of their magnetic susceptibility in response to applied stresses.

MEASUREMENT TECHNIQUES

Unimorph for Measuring Magnetostriction

Since MNMs usually have rough and flexible surfaces, the use of a strain gage for direct measurements of magnetostriction is infeasible even under direct current (DC) magnetic field. In fact, the attachment of the strain gage will affect the MNM flexibility and will interfere accurate strain measurements. Optical methods, such as the use of fiber Bragg gratings (FBGs), can be highly sensitive but require embedding the device in a thick layer of MNM. Video recording of the MNM expansion by monitoring the separation of markings on MNM has sensitivity limited by the resolution of the camera. For enhancing the sensitivity in detecting magnetostrictive strain with the camera, unimorph films with a bilayer of MNM and CNF functioning as actuators were fabricated and used to quantify magnetostriction indirectly. Similar to their counterpart in, piezoelectricity (Smits et al., 1991; Wang and Cross, 1998), their angles of bending or rotation θ are proportional to material parameters and the applied magnetic field $\vec{H}$ (**Figure 1**).

Generally, the magnetomechanical coupling among the normal and shear strains, magnetic flux density, normal and shear stresses and magnetic field intensity is a tensor relation that can be represented by a 9×9 matrix (Elhajjar et al., 2013). Owing to the crystal symmetry, three independent magnetostrictive strain constants d_{13}, d_{33} and d_{15} are dominant. Under quasi-static loading conditions, without prestress, the linearized constitutive stress-strain relationship that models the magnetomechical coupling is further reduced to one magnetostrictive strain constant d_{33}. Particularly for the unimorph film shown in **Figure 1** with a length of L, a CNF thickness of h_{CNF} and a MNM thickness of h_{MNM}, the axial strain along z direction can be obtained from constituent equations:

$$\epsilon_{33} = E_{MNM}^{-1}\,\sigma_{33} + d_{33}\,H_3 \text{ in the MNM layer} \quad (1a)$$

and

$$\epsilon_{33} = E_{CNF}^{-1}\,\sigma_{33} \text{ in the CNF layer} \quad (1b)$$

where the indexing notation for the subscript with 1 for x, 2 for y and 3 for z is used. In Eqs (1a) and (1b), all parameters, including the magnetostrictive strain constant d_{33}, axial stress σ_{33}, magnetic field intensity H_3, Young's modulus of CNF E_{CNF} and Young's modulus of MNM E_{MNM}, refer to the axial component along z. E_{MNM} is established with a unit cell approach (Ravichandran, 1994):

$$E_{MNM} = \frac{\left(E_{TD}E_{CNF} + E_{CNF}^2\,(1+\zeta)^2 - E_{CNF}^2\right)(1+\zeta)}{(E_{TD}-E_{CNF})\,\zeta + E_{CNF}\,(1+\zeta)^2} \quad (2)$$

where $\zeta = \left(\frac{1}{VF_{TD}}\right)^{\frac{1}{3}} - 1$ is a parameter depending on the ratio of the linear dimension of the CNF matrix to the Terfenol-D

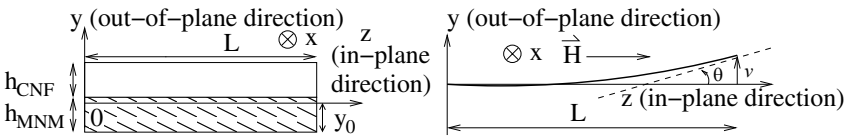

FIGURE 1 | Original dimensions of the unimorph film **(left)** and bending of the unimorph with an angle of rotation θ under magnetic field $\vec{H}$ **(right)**. The in-plane and out-of-plane directions for particle alignment are indicated for this setup.

particle, VF_{TD} is the Terfenol-D volume fraction and E_{TD} is the Young's modulus of Terfenol-D. With the procedure similar to that of piezoelectric unimorph (Wang and Cross, 1998), an expression for the upward θ can be derived for the unimorph film in **Figure 1**:

$$\theta = \frac{d_{33}H_{33}L}{h_{CNF}} \frac{6A\ B\ (1+B)}{A^2\ B^4 + 2A\left(2B\ + 2B^3 + 3B^2\right) + 1} \quad (3)$$

where $A = \frac{E_{MNM}}{E_{CNF}}$ is the Young's modulus ratio, $B = \frac{h_{MNM}}{h_{CNF}}$ is the layer thicknes ratio and $C = \frac{\rho_{MNM}}{\rho_{CNF}}$ is the mass density ratio. θ relates to deflection v or normalized deflection $\delta = \frac{v}{L}$ by

$$\delta = \frac{\theta}{2} \quad (4)$$

Obviously, experimental data of δ can be used to estimate d_{33} with Eq. (4). If the unimorph film is flipped upside down (i.e., rotated 180° about the z-axis), the downward θ will become negative and an expression similar to Eq. (3) can be obtained with the same procedure, except that all parameters (A, B and C) are replaced by their reciprocal values ($A^{'}$, $B^{'}$ and $C^{'}$) and h_{CNF} is replaced by h_{MNM}:

$$\theta = -\frac{d_{33}H_{33}L}{h_{MNM}} \frac{6A^{'}B^{'}\left(1+B^{'}\right)}{A^{'2}\ B^{'4} + 2A^{'}\left(2B^{'} + 2B^{'3} + 3B^{'2}\right) + 1} \quad (5)$$

Clearly, estimated d_{33} values with Eqs (4) and (5) are not purely the property of the MNM but rather is the result of the MNM magnetostriction and the unimorph structure. They serve as indicators for the tendency of MNM response and most importantly demonstrate the application of MNMs as actuators.

Toroidal Coil for Measuring Villari Effect

The probe for the measurement of Villari effect consists of a toroidal coil with a silicon steel core that has a high magnetic susceptibility χ_m, a cross section of $a \times t$ and a short air gap of length l_g (**Figure 2**). The inductance L_m of the probe with a MNM sample under test of thickness d placed within the air gap is recorded with an inductance meter (Al-Hajjeh et al., 2016) and can be calculated with

$$L_m = \frac{N^2\mu_o t\ a}{l_g}\left(\chi_m + \ 1\right) + L_s \quad (6)$$

where N is the number of turns in the coil, μ_o is the permeability of free space, L_s is the series inductance caused by the core and air gaps between the core and MNM. Since $d \cong l_g$ and permeability

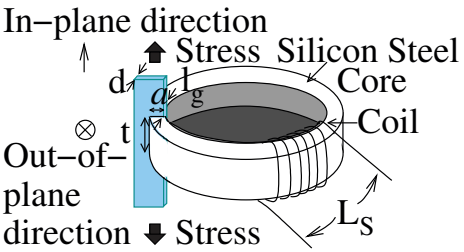

FIGURE 2 | Toroidal coil with a l_g long air gap filled with a MNM sample of thickness d. The in-plane and out-of-plane directions for particle alignment are indicated for this setup.

of silicon steel is large, L_s can be safely neglected and in fact, is canceled in the calculation of the percentage change in magnetic susceptibility:

$$\Delta\chi_m = \frac{L_\sigma - L_a}{L_0 - L_a} \times 100\% \quad (7)$$

where L_σ is the value of L_m at stress $\sigma \neq 0$, L_0 is the value of L_m at $\sigma = 0$ and L_a is the value of L_m at $\chi_m = 0$, i.e., the air gap being empty.

EXPERIMENTAL PREPARATION AND PROCEDURE

Cellulose Nanofibril Production

Cellulose nanofibers (**Figure 3**) were prepared with a TEMPO (tetramethylpiperidine-1-oxy radical)-mediated oxidation pre-treatment according to a procedure described previously (Saito et al., 2007) except here a carbonate buffer system was used to keep the reaction conditions at pH 10. Fully bleached Kraft Eucalyptus fibers were mixed in a pulper at 8% solids then pre-treated with sodium chlorite for 2 h at pH 2 and 2% solids. The pre-treated pulp was then filtered and washed. The washed pulp (1.25 kg) was added to 350 L solution containing 600 g of sodium carbonate and stirred for 1 h in a glass-lined reactor. Sodium bicarbonate (100 g), sodium bromide (120 g), and TEMPO (20 g) were added and dissolved. Finally a solution of sodium hypochlorite (6.2 liter of 8wt%, 5 mol/kg diluted to 20 L) was added, and the reaction was heated to 30°C and stirred overnight. The carboxylated pulp was then filtered, washed and refined in a disk refiner, followed by a single pass through an M-110EH-30 Microfluidizer (Microfluidics, Newton, MA, United States)

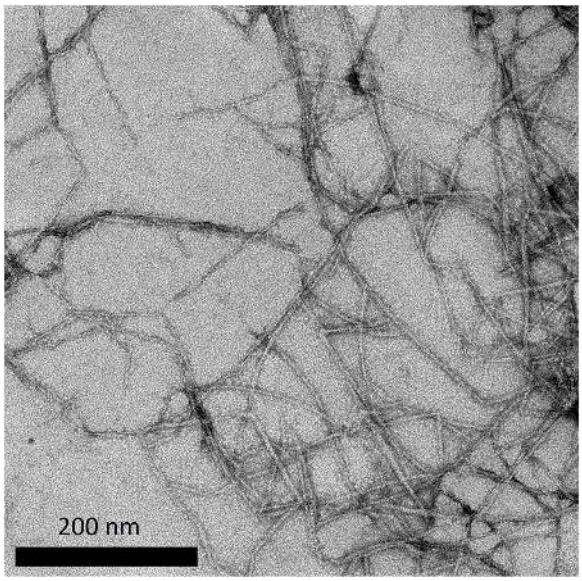

FIGURE 3 | TEM nanograph of CNF nanofibril structure.

with 200- and 87-μm chambers in series at about 1% solids. The carboxyl content of the TEMPO-oxidized CNFs was determined to be approximately 0.8 mmol/g according to TAPPI T237 cm-98 (TAPPI, 2008).

CNF/Terfenol-D Composite Production

Single layer films are MNMs fabricated by mixing an aqueous CNF dispersion with a quantity of 250–300 μm Terfenol-D particles (commercially available from TdVib LLC, formerly Etrema Products), corresponding to a 30% volume fraction. The size specification defines the longest dimension of irregularly-shaped particles. This particle size range was used because prior research has shown that relatively large particles with a narrow size distribution tend to exhibit the best magnetostrictive responses in two phase composites containing Terfenol-D (Rodríguez et al., 2009). While MNMs with higher VF_{TD} have stronger magnetostriction, their flexibilities are reduced. VF_{TD} of 30% was determined to be the optimal value for maintaining both properties. The particles were added and blended into CNF dispersions of approximately 1 wt% solids with an electric impeller mixer. The viscous nature of the CNF dispersion prevented rapid settling of the Terfenol-D particles. The suspensions were then traversed a 142-mm Millipore ultrafiltration system (Millipore Corporation, Billerica, MA, United States) that consisted of filter paper membranes with pore size of 0.1 μm (JVWP14225, JV, Millipore Corporation, United States). The filtration system was sealed and pressurized under 0.55 MPa of air pressure. Once most of the water was extracted and the films were able to be handled, they were removed from the filter system and dried. The final drying procedure entailed first placing the films between an assembly of waxy coated papers and absorbent blotter paper. The stack was placed atop a bed of silica gel desiccant beads, and pressed under a load of approximately 100 N for 24 h. The completed films were stored in a container with desiccant until used in an experiment, whereupon they were allowed to normalize in the experimental space for 24 h prior to testing.

Unimorph films were made by first creating a single MNM layer as described above, and adding CNFs for a second pure layer above the MNM layer by the same procedure. The CNF-Terfenol-D mixture was not allowed to completely dry before adding the second layer. The filtration apparatus was once again pressurized and the water forced out through the filter membrane. When the bulk of the water introduced from the pure CNF suspension was removed, the unimorph hydrogel was dried following the single layer procedure.

Trilayer films were created in similar fashion to the unimorph films, with two CNF-only layers sandwiching the MNM layer. Again, the next layer was deposited before the fully drying of the previous layer. Drying was carried out as described for the single layer samples.

Particle alignment significantly improves the response of magnetostrictive composites, with a correlation between higher aligning field magnitudes and increasing response improvement (Rodríguez et al., 2008). Samples with aligned Terfenol-D particles were created for single layer, unimorph and trilayer MNMs. Two alignment schemes were implemented for each configuration.

In-plane particle alignment was achieved using a laboratory electromagnet. To accomplish this, a plastic containment ring was placed inside the ultrafiltration apparatus, and the CNF/Terfenol-D suspension poured inside of it. For the single layer and unimorph MNMs, the ring sat directly atop the filter membrane. For the trilayer MNM, the ring was atop the partially dried first layer. The filter stack, containment ring and suspension were then carefully removed from the ultrafiltration apparatus, and placed atop a piece of polycarbonate flat stock. The ring was gently clamped down using bar clamps, the entire assembly was placed inside the airgap of the electromagnet and exposed to a 250 Oe (20 kA/m) DC magnetic field for 5 min. The use of low field was critical since Terfeonol-D particles could be separated from the mixture under a high field. This step resulted in pseudofibrous ordering of the particles inside the slurry (**Figure 4a**). The assembly was taken from the electromagnet and unclamped, and the filters, containment ring and suspension carefully transferred

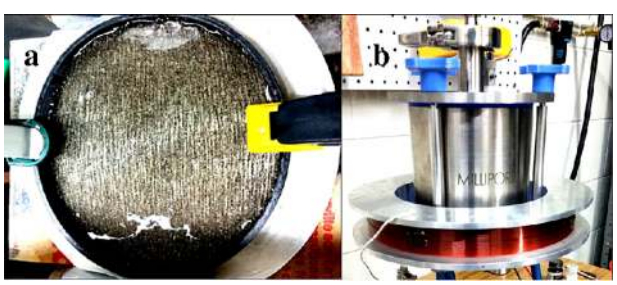

FIGURE 4 | Method of in-plane **(a)** and out-of-plane **(b)** particle alignment of Terfenol-D/CNF MNMs.

back into the ultrafiltration apparatus while taking care to avoid disturbing the particle alignment. The containment ring was lifted out of the apparatus, and the rest of the sample preparation carried out as usual. When the partially dried final sample was removed from the apparatus at the end of filtering, the wax paper/blotter pad/sample stack was gently clamped between two aluminum plates. For further reinforcement of the alignment, this assembly was again placed into the air gap of the electromagnet, and exposed to a higher [3 kOe (239 kA/m)] DC magnetic field for 1 h. The sample was then removed and dried as usual.

Out-of-plane alignment was performed using a solenoid mounted axially on the ultrafiltration apparatus (**Figure 4b**). The solenoid was energized to provide a 250 Oe (20 kA/m) DC magnetic field prior to pressurization, and this field was maintained for the duration of the filtration procedure in order to avoid hydraulic forces undoing the particle alignment. The rest of the procedure was performed as usual. Owing to the limited field from the solenoid, the reinforcement of particle alignments could not be performed at the later stage.

All composite samples, including unimorph and trilayer films) were originally fabricated in forms of disks as shown in **Figure 4a**. Rectangular stripes with uniform dimensions were cut from the center of the disk in order to maintain consistent alignment throughout each sample. These samples were applied to the configurations shown in **Figures 1**, **2**. Notice that the long edge of the film is the alignment direction for the in-plane alignment sample while the thickness of the film is the alignment direction for the out-of-plane alignment sample.

Micro-Structured Active Films

The morphology of unimorph samples resulting from particle alignment were explored via scanning electron microscopy (SEM). Samples were prepared by cryogenic fracturing in order to best preserve features. Each sample was immersed in liquid nitrogen for 20 s and then cleaved apart immediately after removal. The in-plane aligned sample was fractured along the alignment direction. Samples were sputter coated with a gold/palladium alloy at 45 mA (Desk II, Denton Vacuum LLC, United States). Images were then captured at 15 kV accelerating voltage using a SEM (JSM-6460LV, JEOL USA, Inc., United States).

Magnetostrictive Effect

A number of complications existed in the determination of magnetostrictive response of the MNMs. First, the axial strain of the composite was expected to be significantly lower than that of monolithic Terfenol-D. Additionally, the relatively rough surface resulting from inclusion of particles precluded application of traditional strain measurement techniques. For this reason, magnetostrictive response was tested using a non-contact method with unimorph samples whose bending deformation mode would exhibit a greater measurable displacement. The magnetostrictive deflections of four unimorph samples were determined via video extensometry using a digital optical microscope and DC magnetic fields inside a laboratory electromagnet (**Figure 5**). Three samples containing Terfenol-D with random, in-plane and out-of-plane particle alignment were tested, as well as

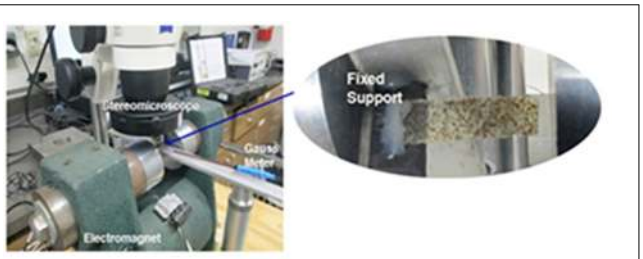

FIGURE 5 | Setup for measuring magnetostrictive response.

one containing 250–300 μm ferrite particles (68 Material, Fair-Rite Products Corporation, United States) with random alignment. These particles were selected due to the similarity of their initial DC magnetic permeability to that of Terfenol-D, but a much smaller magnetomechanical coupling. As such, they would experience similar magnetic attraction but negligible magnetostriction on the order of a few ppm (Bienkowski and Kulikowski, 1980, 1991).

Relative humidity measurements were taken before each trial, with values ranging from 45 to 50%. The electromagnet was placed atop an optical table to damp ambient vibrations from affecting the experiment. An optical microscope (Stemi 2000-C, Carl Zeiss AG, Germany) equipped with a digital camera (AxioCam ICc 1, Carl Zeiss AG, Germany) was mounted to the electromagnet for the purpose of non-contact displacement measurement. Each unimorph sample was cut to uniform rectangular dimensions of 13.5 mm × 40 mm and attached to a 3D-printed slotted holder, designed for a slight interference fit. It is important to note that it was difficult to directly measure the thickness of the film due to the rough surface caused by relatively large Terfenol-D particles. As such, an additional film was created which contained identical amounts of CNF in both layers, but without any particles. This film had an average thickness of 0.261 mm. A black and white grating pattern was painted along the tip of both edges of each sample. The samples were then cantilevered within the center of the electromagnet air gap, with length direction along the central axis of the pole pieces.

Ten cycles of a low frequency alternating current (AC) magnetic field were applied to each sample in order to relax any residual stresses from the mounting procedure. DC current was supplied to the electromagnet to step the magnetic field strength in increments of 200 Oe (15.9 kA/m), completing a full loop with minimum and maximum magnetic field strengths of −2 kOe (-159 kA/m) and 2 kOe (159 kA/m), respectively. An optical microscope image of the sample was captured at each increment. The image sequence obtained was then converted to a video file, and the deflection of the sample as a function of magnetic field strength was extracted by tracking the painted-on grating with open source video analysis software (Tracker Video Analysis and Modelling Tool, Douglas Brown). The process was repeated for each sample flipped over in its holder, and its other edge in view of the microscope. A total of five trials were performed for each sample in each orientation.

Villari Effect

The Villari response of the MNMs was determined by measuring the percentage change in their magnetic susceptibilities $\Delta\chi_m$ as a function of applied tensile stress σ, as reported previously for a magnetostrictive composite stress sensor (Al-Hajjeh et al., 2016). The construction and principle of the probe for measuring Villari response were discussed in Section "Toroidal Coil for Measuring Villari Effect." Here, the special process for sample preparation was described.

Samples were carefully cut and bonded to carbon fiber standoffs which, due to their length and non-ferrous composition, minimized influence of ferromagnetic components in various surrounding apparatus on the magnetic susceptibility reading. Single and trilayer samples with random, in-plane and out-of-plane particle alignment were tested. Additionally, a single layer control sample containing randomly aligned 250–300 μm ferrite particles was tested.

Relative humidity measurements were taken before each trial, with values ranging from 25 to 40%. Each sample was placed in the grips of a load frame (3369, Instron, United States). The probe was mounted such that the sample fully occupied its air gap. A stepped load profile was applied so that the sample experienced tensile stresses from 0 to 25 MPa in 2.5 MPa increments. Load corresponding to each stress step was held for 20 s, with inter-step loading rate corresponding to 0.25 MPa per second. During the loading procedure, inductance of the pickup coil was recorded in NI LabVIEW via an LCR meter (889A, B&K Precision Corporation, United States). Inductance measurements were carried out at 1 V and 100 Hz. Each sample underwent five trials, with the probe moved to a different position on the sample for each trial in order to account non-ideal particle distribution.

It is important to note that the cross sectional area of each sample type was used when setting the load profile. An average width was measured for single and trilayer samples of all particle orientations. Due to the rough sample surface caused by relatively large particles, it was difficult to directly measure film thicknesses. As such, film thicknesses were determined from particle-free samples made using the procedure for the unimorph bending experiment. The single and trilayer samples had average thicknesses of 0.134 and 0.407 mm, respectively. These estimates are consistent with that of unimorph sample and indicate that each layer is about 0.13 mm on average. Owing to the variation in Terfenol-D particle packing density, the estimate of the trilayer film is almost 50% less than that of the SEM micrographs for the sample with in-plane alignment in **Figure 6**.

RESULTS AND DISCUSSION

Morphology

A few images representative of the sample morphologies observed with SEM are shown in **Figure 6**. The randomly aligned sample exhibited a combination of particle clustering and individual particles. Particle wetting was sporadic, with some well-enveloped by the CNF matrix and others surrounded by partial or complete voids.

The in-plane aligned sample exhibited a pseudofibrous structure at the macroscopic scale, with long chains of Terfenol-D particles following the flux lines of the aligning magnetic field. There were no observed instances of individual particles fully wetted by the CNF matrix, with a general trend of well-enveloped clusters of particles instead. Void content for this sample was significantly lower than the other two composite types. The out-of-plane aligned sample displayed a significant increase in apparent void content, to the point where long interlaminar fissures were present in the majority of the imaged cross-section. As with the randomly aligned sample, the particles showed variable levels of wetting by the CNF, and there was a notable reduction in particle clustering. A more frequent incidence of particles aligned spatially out-of-plane was noted relative to the randomly oriented sample. Though it is impossible to pinpoint an exact cause, it is likely that the interlaminar fissures resulted from a combination of particle alignment, viscosity of the CNF, and increased outgassing of entrained air from the CNF due to heat flux into the ultrafiltration apparatus from the particle alignment solenoid.

Magnetostriction for Actuation

The angular deflection data (**Figure 7**) confirmed in two ways that magnetostriction was the dominant source of deformation in the unimorph composite samples. First, there was virtually no response in the ferrite control sample above the noise floor of the measurement system, which was directly related to CCD noise in the microscope camera. Since the ferrite used in the control has approximately the same initial DC magnetic permeability as that of Terfenol-D, this is also an indicator that magnetic attraction acting on the particles contributes negligibly to the observed deformation. Second, the deflection direction of all Terfenol-D-containing samples switched when the sample was flipped in its holder, indicating that the deflection of the sample was due to axial magnetostrictive strain induced in the active layer of the unimorph structure.

Another important observation to be made from the experimental results is the effect that particle alignment had on the response. With the averages of maximal magnitude of upward and downward angles (|θ|) 0.46, 0.86, and 0.12° for the random, in-plane and out-of-plane particle alignment, respectively, it is evident that planar alignment favorably enhances and out-of-plane alignment significantly attenuates magnetostrictive response. Since |θ| is proportional to $|H|$, its maximum occurs at the highest field at 2 kOe (15.9 kA/m). The maximal values for upward and downward angles were mismatched likely owing to the fact that the samples deformed somewhat when drying, complicating alignment with the electromagnet poles during testing. Typical errors are illustrated by expressing the standard deviation in terms of the percentage of the average (Δ) at this field point. For downward angle, Δ is about 8, 33, and 6% for the random, out-of-plane and in-plane particle alignment, respectively. For upward angle, Δ is about 8.2, 25, and 4.16% for the random, out-of-plane, and in-plane particle alignment, respectively. In the calculation of Δ, two data sets were dropped from the downward angle for the random particle alignment owing to data inconsistency. Usually, Δ is smaller

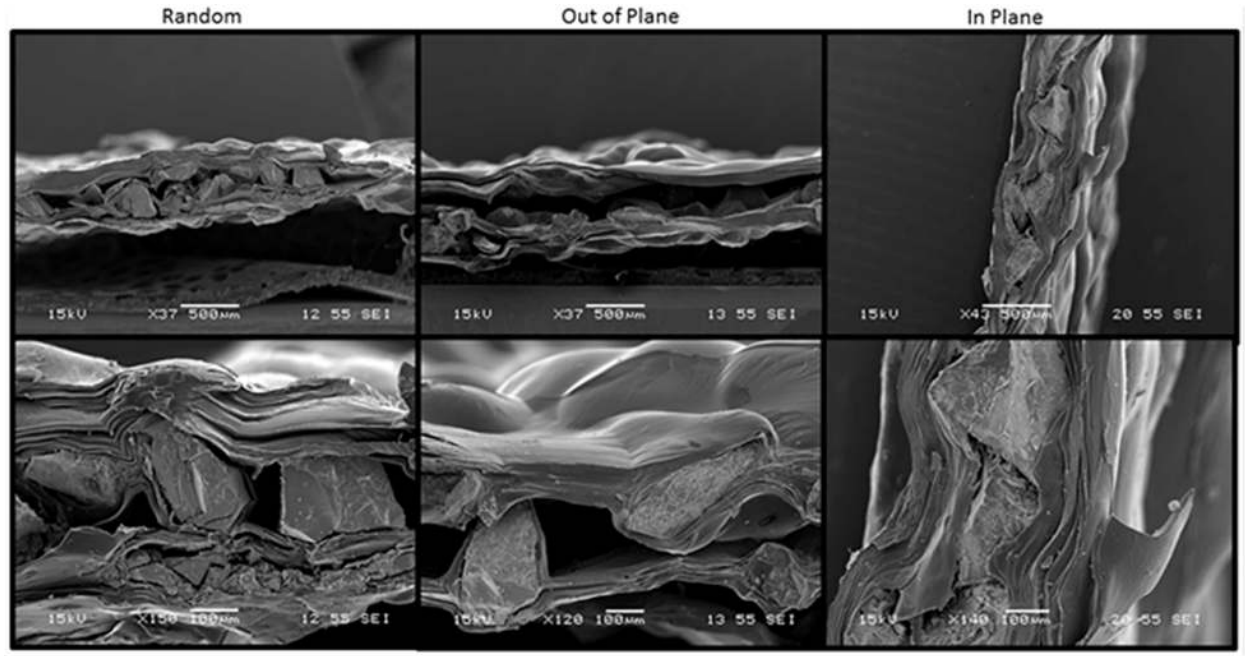

FIGURE 6 | SEM micrographs of trilayer CNF/Terfenol-D samples with random, out-of-plane and in-plane particle alignment.

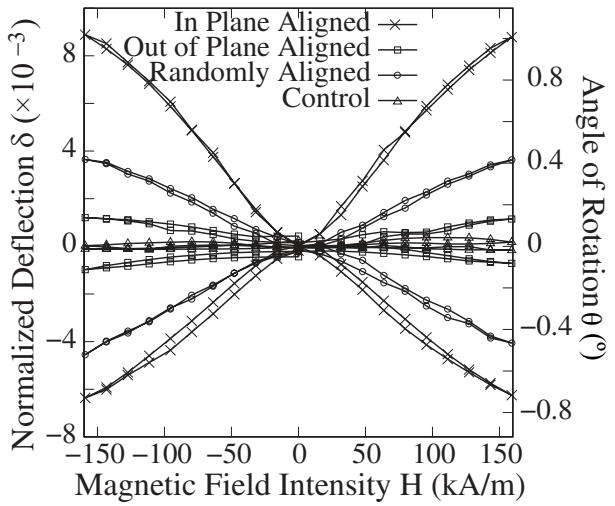

FIGURE 7 | Angle of rotation (normalized deflection) of unimorph films versus magnetic field (curves with $\delta > 0$ and those with $\delta < 0$ corresponding to films oriented in **Figure 1** and flipped version of **Figure 1** respectively).

when the average value is high as illustrated by the smaller Δ for upward angle for out-of-plane and in-plane alignment. Similar trend can be observed at other field points. Addition error should be considered for the different angles under increasing and decreasing field (indicated by arrows in **Figure 7**) owing to hysteresis.

The superior performance of the in-plane aligned sample may be attributable to the morphology difference observed with SEM. The long chains of particles are likely critical to this in two capacities. First, they serve as enhanced magnetic flux paths relative to regions with discontinuous particle content, enhancing the local magnetic flux density. Due to the low relative permeability of Terfenol-D this effect is likely limited. Second, the particles are able to transfer strain to one another directly, potentially increasing the total strain transferred to the CNF matrix and increasing the net magnetomechanical coupling of the composite.

With Eqs (3) and (5), the magnetostrictive strain constant d_{33} is estimated with data from **Figure 7** and plotted as function of H in **Figures 8A,B**. Although d_{33} has the same trend in both figures, the upward bending d_{33} values are consistently larger than those of downward bending, again owing to sample deformations. For example, data for in-plane particle alignment show that maximum d_{33} is 540 pm/A for upward angle and 400 pm/A for downward angle at 1.2 kOe (95.5 kA/m). These values are about one-twentieth of the bulk Terfenol-D value. Typical magnetostrictive strain is assumed to be proportional to $|H|^2$, i.e., d_{33} is a linear function of H, for low field. **Figures 8A,B** validate this assumption for MNM under $|H|$ less than 400 Oe (31.8 kA/m).

Although the estimated d_{33} values for unimorph do not provide the absolute measurement for the magnetstriction in MNM, they present the trend of MNM responses and demonstrate the application of MNM as an actuator. For future investigation, other optical methods, such as measuring the shifts in the spectral response of an FBG (Elhajjar et al., 2013), should be considered for direct measurements of magnetostriction.

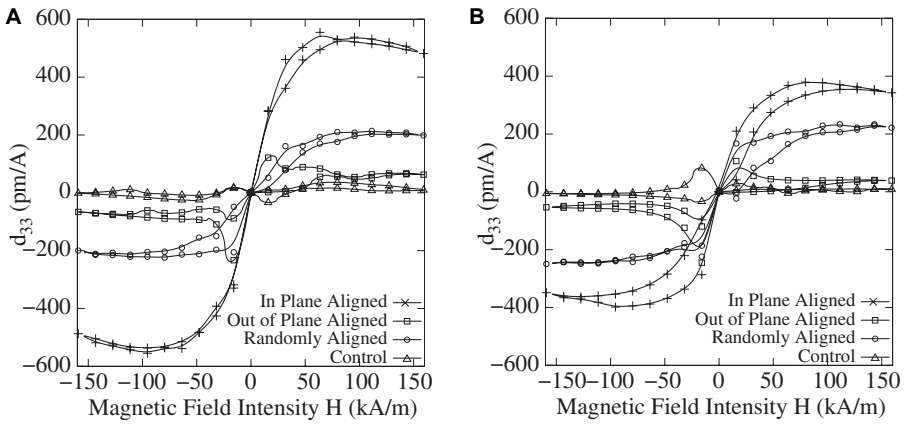

FIGURE 8 | (A) Estimation of d_{33} for unimorph films in **Figure 1** orientation based on data from **Figure 7**. **(B)** Estimation of d_{33} for unimorph films in flipped orientation of **Figure 1** based on data from **Figure 7**.

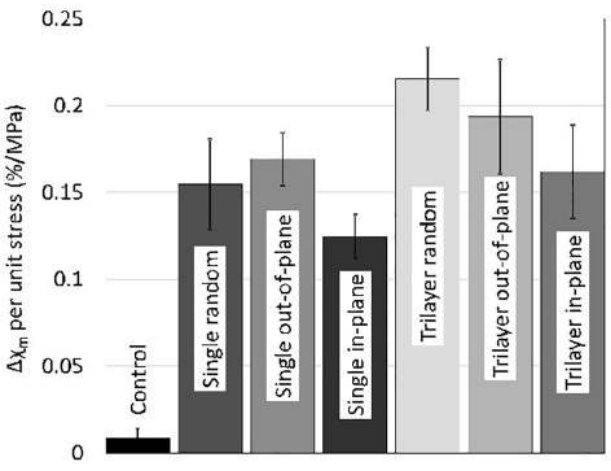

FIGURE 9 | Percentage change in magnetic susceptibility per unit applied stress obtained from the probe configuration in **Figure 2**. The error bars show the variations in response at five locations of each sample measured by the probe that depends on various factors, including the particle distribution and the film thickness. The height of each bar in the histogram shows the expected sensitivity for each sample.

Villari Experiments for Energy Harvesting Potential

With the exception of the control, all samples tested for the Villari effect exhibited highly linear responses over the range of tensile stresses in this experiment (their linearly fitted lines having R-squared values 0.995–0.999). The control sample showed a region of linear increase in magnetic susceptibility, with a peak and reversal at an average stress of 20 MPa. This response characteristic, termed the Villari reversal, is known to occur in NiZn ferrites (Bienkowski and Kulikowski, 1980) and is an indicator that inverse magnetostriction is the primary cause of changes in inductance of the pickup coil.

As indicated in Section "Villari Effect," there were six MNM samples and one control sample. Since the cross section area of the probe is smaller than that of each sample, measurements were performed at five different locations for each sample. This was different from Al-Hajjeh et al. (2016) where magnetostrive composite were completely enclosed by the probe. The average response sensitivities of the samples in terms of percent change in magnetic susceptibility per unit applied stress are presented in **Figure 9**. The average sensitivity should illustrate the general tendency of the response. For instance, the low sensitivity control sample confirms that the response is solely caused by Villari effect, not by other sources for magnetic induction. Similarly, the relatively large error bars, representing one standard deviation, indicate the existence of considerable non-uniformity in the particle distribution and variations in the film thickness. However, a number of observations can still be made.

First, the more sensitive response of the trilayer samples may indicate that the addition of an extra CNF layer on either side of the particle-containing layer improved stress transfer to the Terfenol-D particles, and improved the overall magnetomechanical coupling of the composite. To a certain degree, this result also highlights the problem in strain transfer for the single layer samples that may be the result of voids in the MNM film. Furthermore, the trilayer samples have the additional benefit of CNF, besides protecting the magnetostrictive particles from immediate reaction with the environment and dramatically reducing eddy current losses. It is also expected that these factors will enhance the MNM's dynamic response.

Second, optimally dense and uniform particle distribution appears to be a more critical factor for consistent, high resolution sensing performance of this composite when a localized measurement scheme is used. Hence, this scheme can detect any non-uniformity in a sample.

Finally, the attenuated response in samples with in-plane particle alignment is significant, albeit the large error bars while samples with random and out-of-plane alignments are statistically indistinguishable. It surely indicates that the in-plane alignment should be avoided to achieve better Vallri response.

According to Al-Hajjeh et al. (2016), the composite with an out-of-plane alignment should have highest sensitivity. Although responses from MNM samples are expected to follow the same trend, the current test remains inconclusive in this regard owing to the large variation in responses. This uncertainty seems to illustrate the imperfections in the out-of-plane alignment since the alignment reinforcement is not performed as indicated in Section "CNF/Terfenol-D Composite Production" owing to the difficulty in achieving a high field with a solenoid. Future work for reinforcing Vallri response should be focused on improving the quality of MNM films, e.g., reducing voids, and explore various methods to optimize the out-of-plane alignment, including the use of different alignment directions in sample preparation.

The materials used in this study are expected to be recoverable and recyclable by dissolution and magnetic separation. Although the recyclability of MNMs was not evaluated in this study, such recyclability has been previously demonstrated for cellulose nanomaterial-based solar cells (Zhou et al., 2013, 2014). The ability to recover magnetostrictive materials could thus potentially mitigate the economics and environmental impact of using costly rare earth metals for sensors and energy harvesting devices.

CONCLUSION

The MNM produced with in-plane alignment has the greatest sensitivity to magnetic field for actuation but the lowest performance for stress sensing or energy harvesting applications. Combining relatively large magnetostrictive materials with highly networked biodegradable nanocellulose membranes achieves interesting properties for electronic materials. The materials used are expected to be recoverable. One novelty of our magnetically driven films is the ability to achieve wireless capability making this technology applicable to a wide range of applications. Furthermore, MNMs with additional CNF layers exhibit markedly improved sensitivity in Villari experiments that may attribute to the enhanced stress transfer. Since local variations in particle density are difficult to control, future studies involving a larger scale measurement combined with higher amplitude aligning fields in the out-of-plane direction would be needed for optimization of this material. Further investigation into the effects of magnetostrictive particle size and interfacial bonding with the cellulose nanofibril substrate on the performance of these materials is also warranted as their performance was not optimized in this study.

DATA AVAILABILITY STATEMENT

The datasets generated for this study are available on request to the corresponding author.

AUTHOR CONTRIBUTIONS

AY and AT performed the experiments and data analysis. CL and RE initiated the research idea and developed the theoretical model. CC and RS provided the cellulose nanofibers and assisted in composite fabrication.

FUNDING

AY and AT were supported by the UWM Support for Undergraduate Research Fellows Program. RE and CL acknowledged the support from the UWM Research Growth Initiative Program.

ACKNOWLEDGMENTS

The authors sincerely thank Rick Reiner of the USDA Forest Service Forest Products Laboratory for producing the cellulose nanofibrils and Rahim Reshadi of the University of Wisconsin–Milwaukee (UWM) Structures laboratory for equipment setup.

REFERENCES

Al-Hajjeh, A., Lynch, E., Law, C. T., and El-Hajjar, R. (2016). Characteristics of a magnetostrictive composite stress sensor. *IEEE Magn. Lett.* 7, 1–4. doi: 10.1109/LMAG.2016.2540613

Anton, E.-M., Jo, W., Damjanovic, D., and Rodel, J. (2011). Determination of Depolarization Temperature of (Bi1/2Na1/2)TiO3-Based Lead-Free Piezoceramics. *J. Appl. Phys.* 110:094108. doi: 10.1063/1.3660253

Bienkowski, A., and Kulikowski, J. (1980). The magneto-elastic villari effect in ferrites. *J. Magn. Magn. Mater.* 19, 120–122. doi: 10.1016/0304-8853(80)90570-3

Bienkowski, A., and Kulikowski, J. (1991). Effect of stresses on the magnetostriction of Ni-Zn(Co) ferrites. *J. Magn. Magn. Meter.* 101, 122–124. doi: 10.1016/0304-8853(91)90700-K

Bove, T., Liang, K., and Wolny, W. (2012). "Experimental Study of Temperature & Pressure Effects on High-Porosity PZT Materials," in *Proceedings of the 2012 IEEE International Ultrasonics Symposium* (Germany: IEEE Press Piscataway), 2506–2509. doi: 10.1109/ULTSYM.2012.0627

Chia, C. H., Zakaria, S., Nguyen, K. L., and Abdullah, M. (2008). Utilisation of unbleached kenaf fibers for the preparation of magnetic paper. *Indus. Crops Products* 28, 333–339. doi: 10.1016/j.indcrop.2008.03.012

Chia, C. H., Zakaria, S., Nguyen, K. L., Dang, V. Q., and Duong, T. D. (2009). Characterization of magnetic paper using fourier transform infrared spectroscopy. *Mater. Chem. Phys.* 113, 768–772. doi: 10.1016/j.matchemphys.2008.08.059

Claeyssen, F., Lhermet, N., Le Letty, R., and Bouchilloux, P. (1997). Actuators, transducers and motors based on giant magnetostrictive materials. *J. Alloys Compd.* 258, 61–73. doi: 10.1016/S0925-8388(97)00070-4

Duenas, T. A., and Carman, G. P. (2000). Large magnetostrictive response of terfenol- D resin composites (invited). *J. Appl. Phys.* 87, 4696–4701. doi: 10.1063/1.373133

Elhajjar, R., Law, C. T., and Pegoretti, A. (2018). Magnetostrictive polymer composites: recent advances in materials, structures and properties. *Prog. Mater. Sci.* 97, 204–229. doi: 10.1016/j.pmatsci.2018.02.005

Elhajjar, R., Law, C., and Muliana, A. (2013). Design and characterization of magnetostrictive composites. *Smart Compos.* 55–76. doi: 10.1201/b16257

Fenn, R. C., Downer, J. R., Bushko, D. A., Gondhalekar, V., and Ham, N. D. (1996). Terfenol-D driven flaps for helicopter vibration reduction. *Smart Mater. Struct.* 5, doi: 10.1088/0964-1726/5/1/006

Franke, K., Huelz, H., and Weihnacht, M. (1998). Stress-induced depolarization in PZT thin films, measured by means of electric force microscopy. *Surf. Sci.* 416, 59–67. doi: 10.1016/S0039-6028(98)00500-7

Goldie, J. H., Gerver, M. J., Oleksy, J., Carman, G. P., and Duenas, T. A. (1999). "Composite Terfenol-D sonar transducers," in *Proceedings Volume 3675, Smart Structures and Materials, 1999: Smart Materials Technologies, Symposium on Smart Structures and Materials* (Newport Beach, CA: SPIE Bellingham), 3612–3675. doi: 10.1117/12.352797

Goodfriend, M. J., and Shoop, K. M. (1992). Adaptive Characteristics of the Magnetostrictive Alloy, Terfenol-D, for Active Vibration Control. *J. Intell. Mater. Syst. Struct.* 3, 245–254. doi: 10.1177/1045389X9200300204

Gruverman, A., Auciello, O., and Tokumoto, H. (1996). Nanoscale investigation of fatigue effects in Pb(Zr,Ti)O3 films. *Appl. Phys. Lett.* 69, 3191–3193. doi: 10.1063/1.117957

Jiang, Q. Y., and Cross, L. E. (1993). Effects of porosity on electric fatigue behaviour in PLZT and PZT ferroelectric ceramics. *J. Mater. Sci.* 28, 4536–4543. doi: 10.1007/BF01154968

Li, P., Wen, Y., Liu, P., Li, X., and Jia, C. (2010). A magnetoelectric energy harvester and management circuit for wireless sensor network. *Sens. Actuators A Phys.* 157, 100–106. doi: 10.1016/j.sna.2009.11.007

Moffett, M. B., Clark, A. E., Wun-Fogle, M., Linberg, J., Teter, J. P., and McLaughlin, E. A. (1991). Characterization of Terfenol-D for magnetostrictive transducers. *J. Acoust. Soc. Am.* 89, 1448–1455. doi: 10.1121/1.400678

Moon, R. J., Martini, A., Nairn, J., Simonsen, J., and Youngblood, J. (2011). Cellulose nanomaterials review: structure{,} properties and nanocomposites. *Chem. Soc. Rev.* 40, 3941–3994. doi: 10.1039/C0CS00108B

Moon, S.-J., Lim, C. W., Kim, B. H., and Park, Y. (2007). Structural vibration control using linear magnetostrictive actuators. *J. Sound Vib.* 302, 875–891. doi: 10.1016/j.jsv.2006.12.023

Olabi, A. G., and Grunwald, A. (2008). Design and application of magnetostrictive materials. *Mater. Eng.* 29, 469–483. doi: 10.1016/j.matdes.2006.12.016

Olsson, R. T., Samir, A., Salazar-Alvarez, M. A. S., Belova, , G., Ström, L., Berglund, V., et al. (2010). Making flexible magnetic aerogels and stiff magnetic nanopaper using cellulose nanofibrils as templates. *Nat. Nanotechnol.* 5, 584–588. doi: 10.1038/nnano.2010.155

Qamhia, I. I., Sabo, R. C., and Elhajjar, R. F. (2013). Static and dynamic characterization of cellulose nanofibril scaffold-based composites. *Bioresources* 9.

Qing, Y., Sabo, R., Zhu, J. Y., Agarwal, U., Cai, Z., and Wu, Y. (2013). A comparative study of cellulose nanofibrils disintegrated via multiple processing approaches. *Carbohydr. Polym.* 97, 226–234. doi: 10.1016/j.carbpol.2013.04.086

Ravichandran, K. S. (1994). Elastic properties of two-phase composites. *J. Am. Ceram. Soc.* 77, 1178–1184. doi: 10.1111/j.1151-2916.1994.tb05390.x

Richards, C. D., Anderson, M. J., Bahr, D. F., and Richards, R. F. (2004). Efficiency of energy conversion for devices containing a piezoelectric component. *J. Micromech. Microeng.* 14, 717–721. doi: 10.1088/0960-1317/14/5/009

Rodríguez, C., Barrio, A., Orue, I., Vilas, J. L., León, L. M., Barandiarán, J. M., et al. (2008). High magnetostriction polymer-bonded Terfenol-D composites. *Sens. Actuators A Phys.* 142, 538–541. doi: 10.1016/j.sna.2007.05.021

Rodríguez, C., Rodriguez, M., Orue, I., Vilas, J. L., Barandiarán, J. M., Gubieda, M. L. F., et al. (2009). New elastomer–Terfenol-D magnetostrictive composites. *Sens. Actuators* 149, 251–254. doi: 10.1016/j.sna.2008.11.026

Roundy, S., Wright, P. K., and Rabaey, J. (2003). A study of low level vibrations as a power source for wireless sensor nodes. *Comput. Commun.* 26, 1131–1144. doi: 10.1016/S0140-3664(02)00248-7

Sabo, R., Yermakov, A., Law, C. T., and Elhajjar, R. (2016).). Nanocellulose-enabled electronics, energy harvesting devices, smart materials and sensors: a review. *J. Renew. Mater.* 4, 297–312. doi: 10.7569/JRM.2016.634114

Saito, T., Hirota, M., Tamura, N., Kimura, S., Fukuzumi, H., Heux, L., et al. (2009). Individualization of nano-sized plant cellulose fibrils by direct surface carboxylation using TEMPO catalyst under neutral conditions. *Biomacromolecules* 10, 1992–1996. doi: 10.1021/bm900414t

Saito, T., Kimura, S., Nishiyama, Y., and Isogai, A. (2007). Cellulose nanofibers prepared by TEMPO-mediated oxidation of native cellulose. *Biomacromolecules* 8, 2485–2491. doi: 10.1021/bm0703970

Saito, Y., Takao, H., Tani, T., Nonoyama, T., Takatori, K., Homma, T., et al. (2004). Lead-free piezoceramics. *Nature* 432, 84–87. doi: 10.1038/nature03028

Sehaqui, H., Ezekiel Mushi, N., Morimune, S., Salajkova, M., Nishino, T., and Berglund, L. A. (2012). Cellulose Nanofiber Orientation in Nanopaper and Nanocomposites by Cold Drawing. *ACS Appl. Mater. Interfaces* 4, 1043–1049. doi: 10.1021/am2016766

Siró, I., and Plackett, D. (2010). Microfibrillated cellulose and new nanocomposite materials: a review. *Cellulose* 17, 459–494. doi: 10.1007/s10570-010-9405-y

Small, A. C., and Johnston, J. H. (2009). Novel hybrid materials of magnetic nanoparticles and cellulose fibers. *J. Colloid Interface Sci.* 331, 122–126. doi: 10.1016/j.jcis.2008.11.038

Smits, J. G., Dalke, S. I., and Cooney, T. K. (1991). The constituent equations of piezoelectric bimorphs. *Sens. Actuators A Phys.* 28, 41–61. doi: 10.1016/0924-4247(91)80007-C

Staley, M. E., and Flatau, A. B. (2005). Terfenol-D tooth phone performance characterization and optimization. *J. Appl. Phys.* 97:10R508. doi: 10.1063/1.1855151

TAPPI (2008). *T237 CM-08 Carboxyl Content of Pulp*. Atlanta, GA: Technical Association of the Pulp and Paper Industry. Available at: https://www.tappi.org/publications-standards/standards-methods/standardsonline/

Ueno, T., and Yamada, S. (2011). Performance of energy harvester using iron–gallium alloy in free vibration. *IEEE Trans. Magn.* 47, 2407–2409. doi: 10.1109/TMAG.2011.2158303

Wang, L., and Yuan, F. G. (2008). Vibration energy harvesting by magnetostrictive material. *Smart Mater. Struct.* 17:045009. doi: 10.1088/0964-1726/17/4/045009

Wang, Q.-M., and Cross, L. E. (1998). Performance analysis of piezoelectric cantilever bending actuators AU - Wang. *Qing Ming Ferroelectr.* 215, 187–213. doi: 10.1080/00150199808229562

Wang, T.-Z., and Zhou, Y.-H. (2013). Nonlinear dynamic model with multi-fields coupling effects for giant magnetostrictive actuators. *Int. J. Solids Struct.* 50, 2970–2979. doi: 10.1016/j.ijsolstr.2013.05.012

Zheng, Q., Javadi, A., Sabo, R., Cai, Z., and Gong, S. (2013). Polyvinyl alcohol (PVA)–cellulose nanofibril (CNF)–multiwalled carbon nanotube (MWCNT) hybrid organic aerogels with superior mechanical. *Sci. J.* 3, 20816–20823.

Zheng, X. J., Zhou, Y. C., Liu, J. M., and Li, A. D. (2003). Use of nanomechanical fracture-testing for determining the interfacial adhesion of PZT ferroelectric thin films. *Surf. Coat. Technol.* 176, 67–74. doi: 10.1016/S0257-8972(02)00883-6

Zhou, Y., Fuentes-Hernandez, C., Khan, T. M., Liu, J. C., Hsu, J., Shim, J. W., et al. (2013). Recyclable organic solar cells on cellulose nanocrystal substrates. *Sci. Rep.* 3:1536. doi: 10.1038/srep01536

Zhou, Y., Khan, T., Liu, J. C., Fuentes-Hernandez, C. Won, Shim, J., Najafabadi, E., et al. (2014). Efficient recyclable organic solar cells on cellulose nanocrystal substrates with a conducting polymer top electrode deposited by film-transfer lamination. *Org. Electron.* 15, 661–666. doi: 10.1016/j.orgel.2013.12.018

Conflict of Interest: The authors declare that the research was conducted in the absence of any commercial or financial relationships that could be construed as a potential conflict of interest.